3D metrological shape measurements from X-ray radiographs

Lucie Calmettes, M.L.M. François, Julien Réthoré

▶ **To cite this version:**

Lucie Calmettes, M.L.M. François, Julien Réthoré. 3D metrological shape measurements from X-ray radiographs. 25e Congrès Français de Mécanique, Nantes, Aug 2022, Nantes, France. ⟨hal-04281694⟩

HAL Id: hal-04281694

https://hal.science/hal-04281694v1

Submitted on 13 Nov 2023

HAL is a multi-disciplinary open access archive for the deposit and dissemination of scientific research documents, whether they are published or not. The documents may come from teaching and research institutions in France or abroad, or from public or private research centers.

L'archive ouverte pluridisciplinaire **HAL**, est destinée au dépôt et à la diffusion de documents scientifiques de niveau recherche, publiés ou non, émanant des établissements d'enseignement et de recherche français ou étrangers, des laboratoires publics ou privés.

HAL Authorization

3D metrological shape measurements from X-ray radiographs

Lucie Calmettes[a], Marc François[b], Julien Réthoré[c]

a. GeM, Université de Nantes, UMR 6183 CNRS, lucie.calmettes@etu.univ-nantes.fr
b. GeM, Université de Nantes, UMR 6183 CNRS, Marc.Francois@univ-nantes.fr
c. GeM, Ecole Centrale de Nantes, UMR 6183 CNRS, julien.rethore@ec-nantes.fr

Résumé :

Avec l'essor de l'impression 3D, il est désormais possible de fabriquer des matériaux en treillis dont la structure est composée de poutres, qui sont de très bons candidats pour réaliser des structures légères et solides. Mais cette technologie entraîne des défauts géométriques dans les pièces imprimées. Nous cherchons donc à déterminer la géométrie réelle du treillis imprimé. Pour ce faire, nous explorons les méthodes de tomographie par ordinateur. Contrairement aux méthodes classiques de reconstruction géométrique, l'idée que nous suivons dans cet article est de ne jamais reconstruire la géométrie en voxel à partir des radiographies obtenues avec le tomographe, mais d'exploiter directement ces radiographies pour effectuer la mesure de forme. Les radiographies virtuelles du modèle CAO seront comparées aux radiographies acquises . Le modèle CAO est déformé jusqu'à ce que ses radiographies correspondent à celles obtenues avec le tomographe. Cette méthode reprend la méthode VIC en 3D sous le nom de 3D-VIC, ce qui donne une méthode robuste et efficace pour effectuer une mesure de forme volumétrique 3D à partir de radiographies obtenues avec un tomographe, avec une précision inférieure au pixel.

Abstract :

With the rise of 3D printing, it is now possible to manufacture lattice materials whose structure is composed of beams, which are very good candidates for making lightweight and strong structures. But this technology leads to geometrical defects in the printed parts. We are therefore seeking to determine the actual geometry of the printed lattice. To do so, we explore computed tomography methods. Contrary to conventional geometrical reconstruction methods the idea we follow in this paper is to never reconstruct the geometry in voxel from the radiographs obtained with the tomograph, but to directly exploit these radiographs to perform the shape measurement. Virtual radiographs of the CAD model will be compared with acquired radiographs . The CAD model is deformed until its radiographs match with those obtained with the tomograph. This method will carry the VIC method in 3D as 3D-VIC, this results in a robust and efficient method to perform 3D volumetric shape measurement from X-ray radiographs obtained with a tomograph, with a subpixel accuracy.

Mots clefs : Volume shape measurement, VIC, tomography, Free form deformation

1 Introduction

Computed tomography (CT) is more and more adopted in the non-destructive evaluation community. However, CT is subjected to various errors or artefacts such as noise, beam hardening, scatter, motion blur, metal artifacts [1] accumulated during the reconstruction of the object volume, which leads us to question the metrological nature of the reconstructed volume. Conventional geometrical reconstruction methods first generate a 3D image of the object to be inspected using algebraic reconstruction methods. Then, the printed CAD model is registered on the reconstructed 3D image (in the voxel base), the accuracy of the result depends directly on the quality of the reconstructed image. Proceeding in this way is problematic in relation to the mass of data generated, in fact, to reconstruct, it will be necessary to take into account many unknowns corresponding to the grey level of each voxel. Moreover, volume reconstruction is very time consuming, both during tomography with the need for a very large number of radiographs where acquisition times can range from a few minutes to a few hours but also during the computation of the volume reconstruction [6][4].
The usual reconstruction algorithms used in computed tomography do not take advantage of the fact that the ideal geometry could be known from the CAD model. In our study, when printing a lattice, it is necessary to have a CAD of this object. The aim being to reconstruct the geometry of an object after 3D printing, the CAD can be used as a reference and starting point for the geometrical reconstruction algorithm which will be used.

This paper proposes an iterative algorithm to evaluate the geometry of a structure after 3D printing, this algorithm will be based on the VIC method [9][11] , which aims to compare a virtual image and a real image and to iteratively modify the virtual image until the virtual and real images match together. In this case, the radiographs from the CT scan will be the real images and the digital duplicates from the CAD will be the virtual images. This iterative algorithm will be implemented in several steps described by the figure 1 :

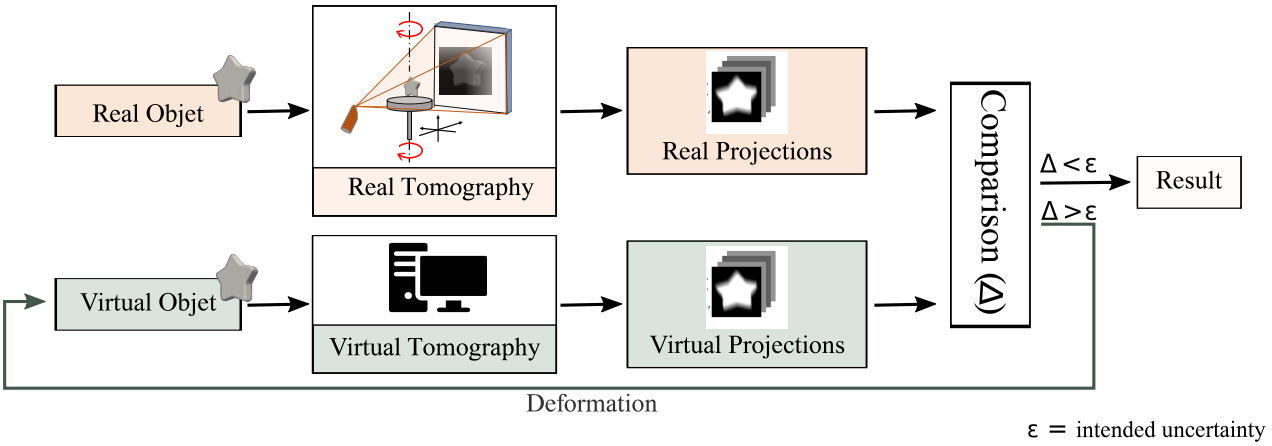

FIGURE 1 – VIC method applied in 3D

1. Creation of virtual CAD radiographs in a virtual tomograph
2. Comparison of virtual and real radiographs and calculation of residual
3. Adjusting of the CAD model if the residual is greater than the desired uncertainty

In a first part, the process of creating the radiographs by rasterization will be described. Then we will explain the calculation of the cost function which allows to calculate the residual between the real and virtual radiographs. Finally, in part 3 we will talk about the Free Form Deformation (FFD) method used to adjust the geometry at each stage of convergence.

2 Creation of virtual CAD radiographs in a virtual tomograph

2.1 Acquisition of data with a tomograph

The idea of our VIC-based method is to create simulated radiographs of the CAD model that match the physical images, which are the radiographs of the object obtained with the tomograph. In this work, the real images are simulated, they have not yet been taken with a tomograph, a digital twin of the tomograph is generated that creates indexed radiographs by θ using the Beer-Lambert law 2 [7]. The Beer-Lambert law relates the sum of the absorption along the path of the x-ray $L(u)$ to the recorded intensity $I(u)$ at each rotation angle $\theta(t)$ at time t, and characterizes a material property of how much the material can attenuate the X-rays for each detector position $u = [y_0, z_0]$:

$$\mathbf{F}_\theta(u) = I_0 exp(-\int_{x \in L(u)} \mu(x) dx) \tag{1}$$

Where I_0 is the blank intensity, μ the absorption coefficient of the material consider steady in time and constant in the material, in this case $\mu(x) = \mu$ and μ no longer depend on x.
. leading to the simplified expression :

$$\mathbf{F}_\theta(u) = I_0 exp(-L(x)\mu) \tag{2}$$

where $L(x)$ is the length that the photon travels in the material. Radiographs will be defined on a gray scale in float numbers between 0 and 1. The next step is to find a numerical method to launch a ray through the mesh of the CAD model and to obtain the distance traveled through it. For this, a rasterization method will be implemented in which the only law of interaction of light with material used will be the absoption, given by the Beer-Lambert law.

2.2 Creation of radiographs by rasterization rendering techniques

The two mains algorithm used in computer graphics are ray-tracing and rasterization. Over the years rasterization became the dominant approach for is low computational requirements, even if handling of global effects such as reflections is intricate [3].
In our application as we are mostly dealing with absorption, so rasterization is a good compromise between fast computing and accuracy of the result, the rasterization was done with algorithm [8], which was provided especially for tomography rasterization.
The idea of the rasterization method is to launch a beam from a source to the mesh. This beam passes through the mesh and impacts on the centre of a detector. This method is decomposed on three steps, the first one is to project the triangle mesh onto a camera plane. The second one is to do the rasterization, it means finds the pixels which are covered by the projected triangle. The last step is to use a z-buffer, the aims is to keep track of the nearest triangle index, in this way, we can update the image value by the nearest triangle to the detector. The z-buffer is a numerical method that allows to record in an array

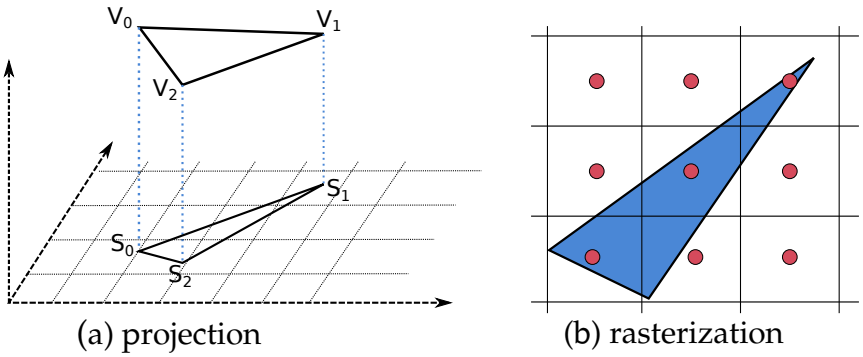

FIGURE 2 – Illustration of rasterization technique. (a) the radiograph step (b) rasterization step which determines the pixel covered by triangle [8]

which triangle is in front of the other one when the X-ray crosses the mesh, and allows to keep a history of the X-ray path into the material.
After the reconstruction of virtual radiographs using this method, they will be compared to the real radiographs obtained during the tomography.

3 Evaluation of virtual radiographs with respect to real radiographs

The idea of the method is to evaluate the difference between the real and virtual radiographs and according to this result, to adapt the geometry of the CAD model. Thus to adapt the CAD model, we will consider that it depends on shape parameters called λ_i. To evaluate the difference between real and virtual radiographs, a cost function Ψ is created, which is defined as the mean square difference in terms of grey levels between real and virtual radiographs respectively $F_\theta(y_0, z_0)$ and $G_\theta(y_0, z_0, \lambda_0, ..., \lambda_n)$, the number of shape parameters is n+1. Thus the Ψ function to be minimized with respect to the λ_i is the following :

$$\Psi(\lambda_0, ..., \lambda_n) = \sum_\theta \int \int (F_\theta(y_0, z_0) - G_\theta(y_0, z_0, \lambda_0, ..., \lambda_n))^2 dy_0 dz_0 \tag{3}$$

Where λ_i are shape parameter corresponding of the control nodes of the morphing box in which the CAD model is embeded, describe in part 4.2. If Ψ is greater than desired discrepancy, a new set of morphing parameters λ_i is computed and virtual radiographs $G_\theta(x_0, y_0, \lambda_i)$ are calculated from the updated CAD model.
When stagnation of the Ψ function is obtained, it means that the virtual and physical radiographs are similar and that we have found the optimal morphing parameters, λ_i describing the geometry of the printed object.

4 Deformation of the CAD model

4.1 Calculation of a new set of parameters

If the residual of the equation 3 is larger than the expected value a new set of CAD shape parameters is calculated with a Newton algorithm. Lets consider Λ_k a vector of the λ_i shape parameter of the CAD model at the k^{th} iteration. The new set of parameters will be calculated as :

$$\Lambda_{k+1} = \Lambda_k - [H_{\Psi(\Lambda_k)}]^{-1} \nabla\Psi(\Lambda_k) \tag{4}$$

Where $H_{\Psi(\Lambda_k)}$ the hessian matrix of Ψ with respect to Λ_k and $\nabla\Psi(\Lambda_k)$ the gradient of Ψ with respect to Λ_k.This new set of parameters Λ_{k+1} is then used to update the CAD model using a Free Form Deformation method.

$$\nabla\Psi(\Lambda_k) = \begin{pmatrix} \frac{\partial\Psi}{\partial\lambda_0} \\ \vdots \\ \frac{\partial\Psi}{\partial\lambda_n} \end{pmatrix}$$

The derivatives are written as :

$$\frac{\partial\Psi(\lambda_0, ..., \lambda_n)}{\partial\lambda_i} = \sum_\theta \int\int -2(F_\theta(y_0, z_0) - G_\theta(y_0, z_0, \lambda_0, ..., \lambda_n)) \frac{\partial G_\theta}{\partial\lambda_i} dy_0 dz_0 \tag{5}$$

$$H_{\Psi(\Lambda_k)} = \begin{pmatrix} \frac{\partial^2\Psi}{\partial{\lambda_0}^2} & \cdots & \frac{\partial^2\Psi}{\partial\lambda_0\lambda_n} \\ \vdots & \ddots & \vdots \\ \frac{\partial^2\Psi}{\partial\lambda_n\lambda_0} & \cdots & \frac{\partial^2\Psi}{\partial{\lambda_n}^2} \end{pmatrix}$$

The second derivatives are written as :

$$\frac{\partial\Psi^2(\lambda_0, ..., \lambda_n)}{\partial\lambda_i^2} = \sum_\theta \int\int 2(-(F_\theta(y_0, z_0) - G_\theta(y_0, z_0, \lambda_0, ..., \lambda_n)) \frac{\partial G_\theta^2}{\partial\lambda_i\partial\lambda_j} + \frac{\partial G_\theta}{\partial\lambda_i}\frac{\partial G_\theta}{\partial\lambda_j}) dy_0 dz_0$$

As in VIC 1D, it has been assumed that the second derivative term is very small and therefore negligible. The second derivative becomes :

$$\frac{\partial\Psi^2}{\partial\lambda_i^2}(\lambda_0, ..., \lambda_n) = \sum_\theta \int\int 2(\frac{\partial G_\theta}{\partial\lambda_i}\frac{\partial G_\theta}{\partial\lambda_j}) dy_0 dz_0 \tag{6}$$

The stopping criterion of the Newton optimization algorithm used will be a stopping criterion in convergence speed, when the value of $\Lambda_k - \Lambda_{k-1}$ will be lower than a certain value ϵ.

4.2 Use of the Free Form Deformation method (FFD) to deform the CAD model

To deform the CAD model, the Free Form Deformation [2][10] method is used. The FFD method principle is to immerse the discretized (using finite elements) CAD model in a simple cuboid box described by B-spline or Bezier curve, knowing that B-splines are the generalization of Bézier curves. B-splines

curves in $\mathbb{R}^d$ are constructed with a linear combination of B-splines basis functions, The coefficients of those basis functions are called control points which are somewhat analogous to nodal coordinates in finit element analysis [5]. B-splines morphing boxes result from a mapping beetween a parametric domain I and a physical space from a set of B-splines functions and the locations of their control points. In this way, a d-dimensional morphing box living in a D-dimensionnal space is defined as :
$S : I \subset \mathbb{R}^d \longrightarrow \mathbb{R}^D$

$$\xi \longmapsto S(\xi) = \sum_{i=1}^{n_{\mathrm{FFD}}} N_i(\xi) {x^*}_i \tag{7}$$

Where $(N_i)_{i=1...n_{\mathrm{FFD}}}$ are the spline functions or bernstein polynomial function associated to the n_{FFD} control point. The idea is to relate the nodal displacements of the mesh to a more regular field defined in the FFD box. After this manipulation, we obtain a parametrization of the CAD model shape adjustment simply driven by moving the control points of the morphing box. In this way, instead of looking for the position of the nodes of the mesh of the geometry we wish to reconstruct, the position of the nodes of the morphing box in which the geometry is immersed will be sought. This reduces the number of degrees of freedom of the problem.

The deformation at one node of the CAD mesh could be written as :

$$u_j = \sum_{i=1}^{n_{\mathrm{FFD}}} N_i({\xi_j}^{FE}) {u^*}_i \tag{8}$$

where u_j is the value of the field at the jth CAD mesh node, n_{FFD} is the number of control points of the morphing box, ${\xi_j}^{FE}$ is the j^{th} mesh node coordinate , ${u^*}_i$ is the value of the field at the ith control point and $(N_i)_{i=1...n_{\mathrm{FFD}}}$ are the spline functions associated to the n_{FFD} control points $({u^*}_i)_{i=1..n_{\mathrm{FFD}}}$[2]. The actual description of the morphing box is done with Bernstein polynomial thanks to PyGem algorithm, which is a python library, to perform the deformation with the FFD method[12].

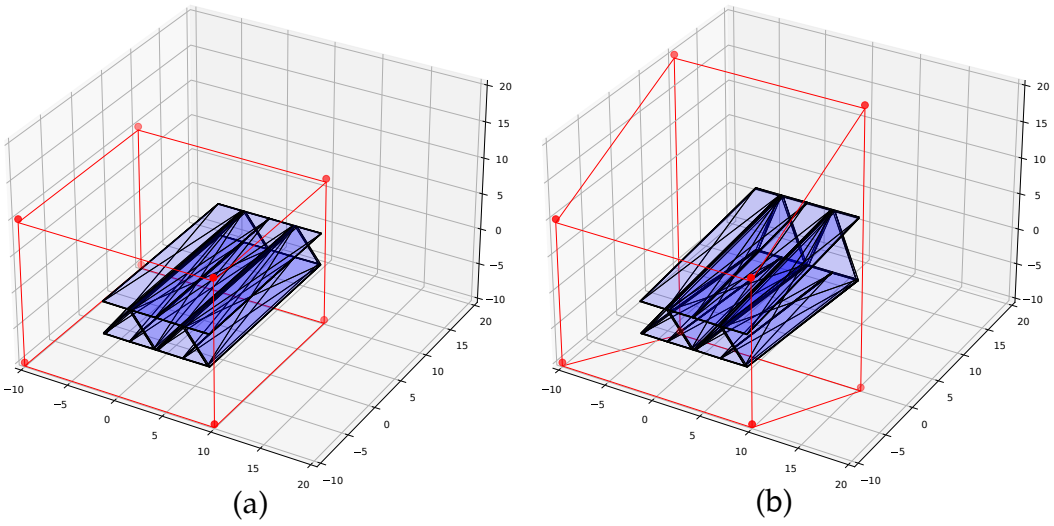

FIGURE 3 – CAD geometry immersed in a morphing box in red (a) the geometry immersed in the morphing box before deformation of the morphing box (b) After deformation of the morphing box

5 Results and perspectives

In this section we will show an example of the use of the described shape correlation algorithm. First, using the FFD method, a lattice was deformed by relocating randomly accordingly to a uniform law between -6mm and 6 mm. The blue geometry in the figure 4 was obtained from the green geometry.

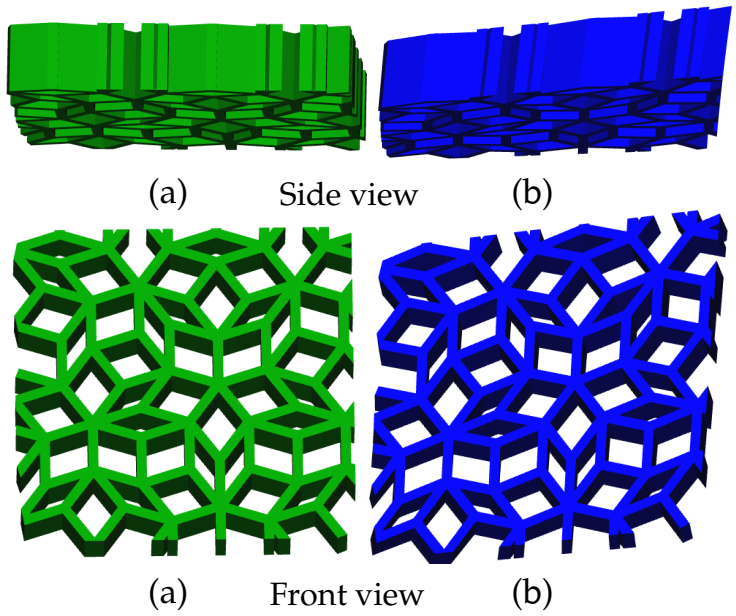

FIGURE 4 – (a) The Initial CAD model (b) the deformed geometry that we try to recover.

The deformed geometry will be the one sought by the algorithm corresponding to some deformation of the object due to 3D printing. With the help of the rasterization algorithm the radiographs from the tomography of the "printed lattice" are calculated, these will be the "real radiographs".

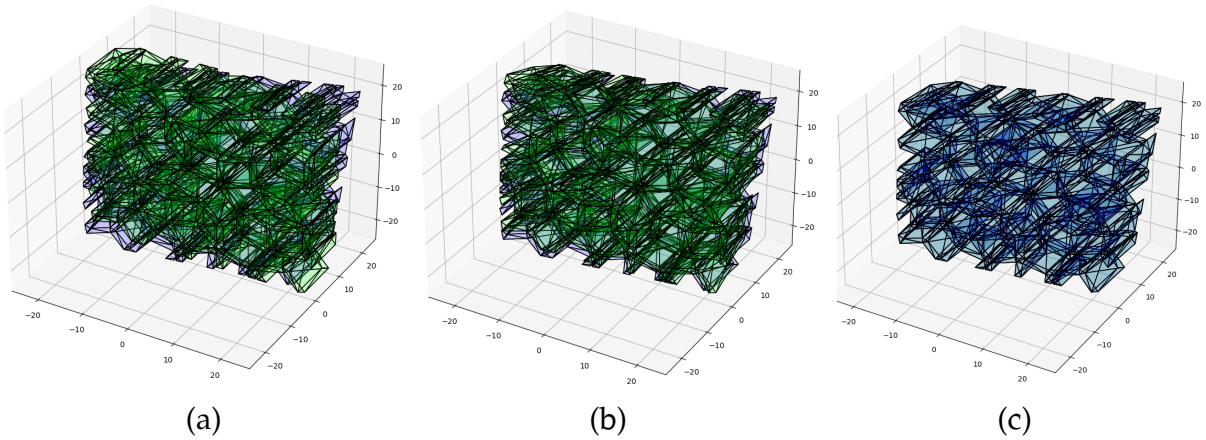

FIGURE 5 – Example of the convergence for a lattice geometry, in green the real geometry of the object we want to find and in blue the virtual CAD geometry. (a) The initial step (b) Iteration 8 (c) Iteration 33 and final step.

The initial geometry used for the search will be the green one corresponding to the CAD model. This one will be iteratively deformed as the convergence progresses by calculating the radiographs from the

CAD model called "virtual radiograph". The figure 8 shows the different stages of this convergence. In this example the convergence was very fast and needed 278 secondes with 33 iterations using a GPU Quadro M2000 with RAM 16 GB. Only 7 radiographs by iterations were used, and 8 control points on the morphing box, to have more local deformation, we could used more control point knowing that adding more control point expend the time computation because of the calculation of the $\nabla\Psi(\Lambda_k)$ the gradient of Ψ with respect to Λ_k. Finally if we calculate the standart deviation of the difference between the real position of the nodes of the mesh and the position found the result is about 0.003 pixem knowing that the criterion to stop the convergence ϵ is equal to 0.00001 mm.

The reconstruction of the geometry was tested with a number of radiographs used ranging from 2 to 20. Here are the results obtained, in order to highlight the impact of the number of radiographs when they are even or odd, on the graphs when the number of radiographs is even the point will be red otherwise it will be green. :

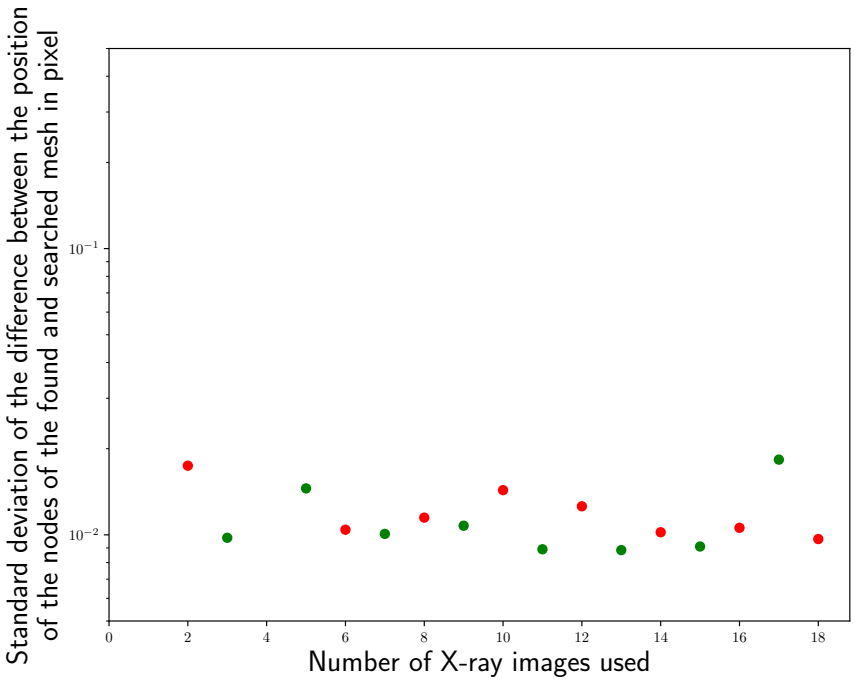

FIGURE 6 – Calculation of the standard deviation of the position difference between the mesh nodes of the reconstructed geometry and the one to be recovered with respect to the number of radiographs

We can notice a difficulty to converge when the number of radiographs is a multiple of two, this can be explained by the symmetry of the geometry used. When we use only an even number of radiographs, namely 4, they are two by two mirroring each other. It is therefore necessary to avoid using a small number of pair radiographs. On the other hand, when an odd number of radiographs is used, one can be satisfied with using a small number, because there is little impact to increase the number of radiographs except to increase the computation time.

In the future, we will realize the deformation from B-spline to perform local deformation. Then real images will be taken to test the algorithm in real situation and evaluate the noise impact, and others experimental bias. With the actual rasterization method on beam correspond to one pixel, to have a better accuracy in the virtual tomography construction, we will discuss about a refinement method in

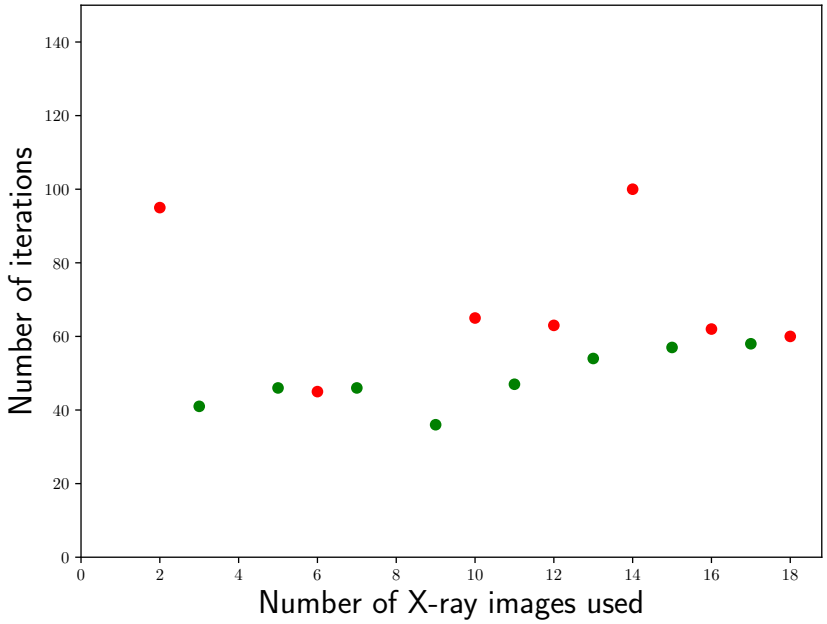

FIGURE 7 – Number of iterations needed to converge with respect to the number of radiographs

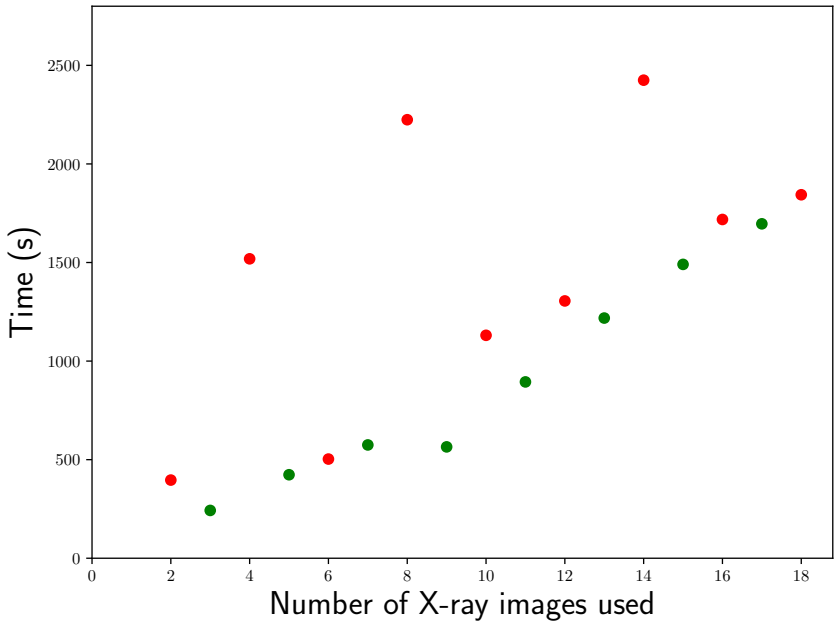

FIGURE 8 – Computation time(s) with respect to the number of radiographs

order to have more than one beam by pixel as done in 2D VIC [9][11] in which a refinement of a factor 3 is commonly used.
Finally, in important part of the work will be to calibrate the virtual tomograph to be able to obtain radiographs similar to the real ones. In this way we decided to make the calibration using directly the 3D VIC algorithm described above, but in this case the supplementary parameters λ_i will correspond to the calibration parameters, i.e. the different characteristic distances in the tomograph, I_0 and the absorption coefficient μ.

6 Conclusion

We are currently able to make simulated radiographs of the CAD for both cone and parallel beam. We will compare real and simulated radiographs using as few radiographs as possible. If the real radiographs are not identical to the simulated radiographs the CAD model will be deformed with a FFD method.
Compared to conventional registration techniques, the proposed approach requires much less radiographs. Further, the expected accuracy is sub-voxel and no biases due to 3D voxel image reconstruction is induced. This results in a robust and efficient VIC-based method to perform 3D volumetric shape measurement from X-ray radiographs obtained with a tomograph.

Références

[1] Franz Edward Boas and Dominik Fleischmann. CT artifacts : causes and reduction techniques. *Imaging in Medicine*, 4(2) :229–240, April 2012.

[2] Morgane Chapelier, Robin Bouclier, and Jean-Charles Passieux. Free-Form Deformation Digital Image Correlation (FFD-DIC) : A non-invasive spline regularization for arbitrary finite element measurements. *Computer Methods in Applied Mechanics and Engineering*, 384 :113992, October 2021.

[3] Tomáš Davidovič, Thomas Engelhardt, Iliyan Georgiev, Philipp Slusallek, and Carsten Dachsbacher. 3D rasterization : A bridge between rasterization and ray casting. pages 201–208, May 2012.

[4] Cédric Fragnaud, Clément Remacha, Julián Betancur, and Stéphane Roux. CAD-based X-ray CT calibration and error compensation. *Measurement Science and Technology*, 2022.

[5] Thomas J.R. Hughes, J. Austin Cottrell, and Yuri Bazilevs. Isogeometric analysis : CAD, finite elements, NURBS, exact geometry and mesh refinement. *Computer Methods in Applied Mechanics and Engineering*, 194(39) :4135–4195, October 2005.

[6] Clement Jailin. Projection-based in-situ 4D mechanical testing. page 241.

[7] Jakeoung Koo. *Tomographic Segmentation from Limited Projection Data*. PhD thesis, Technical University of Denmark, 2021.

[8] Jakeoung Koo, Anders B. Dahl, J. Andreas Bærentzen, Qiongyang Chen, Sara Bals, and Vedrana A. Dahl. Shape from Projections via Differentiable Forward Projector for Computed Tomography. *Ultramicroscopy*, 224 :113239, May 2021. arXiv : 2006.16120.

[9] Julien Réthoré and Marc François. Curve and boundaries measurement using B-splines and virtual images. *Optics and Lasers in Engineering*, 52 :145–155, 2013. Publisher : Elsevier.

[10] Thomas W Sederberg. Free-Form Deformation of Solid Geometric Models. 20(4) :10, 1986.

[11] B. Semin, Harold Auradou, and Marc. François. Accurate measurement of curvilinear shapes by Virtual Image Correlation. *European Physical Journal : Applied Physics*, 56(1) :10701, October 2011. Publisher : EDP Sciences.

[12] Marco Tezzele, Nicola Demo, Andrea Mola, and Gianluigi Rozza. PyGeM : Python Geometrical Morphing. *Software Impacts*, 7 :100047, February 2021.